# A detailed insight into the preparation of nanocrystalline TiO2 powders in supercritical carbon dioxide

Audrey Hertz, M. Drobek, C. Ruiz, F. Charton, S. Sarrade, C. Guizard, A. Julbe

# A detailed insight into the preparation of nanocrystalline $TiO_2$ powders in supercritical carbon dioxide

**A. Hertz[1], M. Drobek[2], J-C. Ruiz[1], F. Charton[1], S. Sarrade[3], C. Guizard[2], A. Julbe[2]**

*[1]CEA, DEN, Marcoule, F30207 Bagnols sur Cèze, France*

*[2]Institut Européen des Membranes, ENSCM-UM-CNRS UMR5635 - Université de Montpellier, Place Eugène Bataillon, 34095 Montpellier cedex 5, France*

*[3]CEA, DEN, Saclay, F91191 Gif-sur-Yvette Cedex, France*

**Abstract:**

This work reports detailed investigations for the preparation of nanostructured titania powders by a solvent-free sol-gel derived process, operated in supercritical $CO_2$ (SC-$CO_2$) at high pressures (10 - 30 MPa) and large range of temperatures (373 K – 823 K). Depending on the processing temperature, the reaction between $Ti(OiPr)_4$ and water performed in a single supercritical phase led to the formation of either amorphous ($Ti(OH)_4$ - Titanium hydroxide) or crystalline ($TiO_2$ – Titania or Titanium dioxide) nanostructured particles. Crystalline (anatase) mesoporous powders with high specific surface area were obtained directly in $CO_2$ solvent under supercritical conditions at temperatures as low as 523 K. The effect of hydrodynamic key process parameters such as stirring and water injection rate on both powder morphology and aggregation degree was also investigated in details. The optimized $TiO_2$ anatase powders exhibited attractive photocatalytic activity, with high potential for the degradation of water pollutants.

**Key-words:** Supercritical $CO_2$; sol-gel route; hydrolysis/condensation reactions; $TiO_2$ nanophased particles; photocatalysis; water and wastewater treatment.

## 1. Introduction

Titania ($TiO_2$) has been historically used in a number of industrial areas including paints, cosmetics and health care products [1]; it is also a key material in photocatalytic applications [2, 3]. Indeed, $TiO_2$ has been found to be an efficient material in environmental clean-up processes to decompose a wide variety of contaminants in both water and air [4, 5]. In addition $TiO_2$ also deserves special attention for photo-electrochemical cell applications, with the recent discovery and developments of solar cells based on dye-sensitized $TiO_2$ photo-electrodes [6]. Most of these applications require $TiO_2$ nanopowders with specific characteristics, namely high specific surface area, large accessible (meso)porosity and the anatase crystalline form.

$TiO_2$ nanopowders can be prepared by various methods, including chemical vapor deposition (CVD) [7], thermal hydrolysis of titanium tetrachloride [8, 9], thermal decomposition/pyrolysis of metal-organic precursors [10-13], and more frequently by sol-gel techniques [14-23]. The latter approach, which can be operated under more or less sophisticated conditions (e.g. ultrasounds, microwaves, pressure…), is a powerful method for the preparation of both titania powders and films. However, classical sol-gel methods often require the utilization of costly and polluting organic solvents and/or chemical additives which have to be eliminated by drying and firing treatments of the final material, thus increasing both the environmental impact and costs of the synthesis process. In addition, the formation of powders with high specific surface area is not straightforward as far as it is often tricky to avoid strong agglomeration of individual particles. Trying to overcome such bottlenecks, the thermal decomposition of titanium alkoxides in supercritical alcohols was reported at the beginning of the 90's as an efficient method to prevent agglomeration: spherical $TiO_2$ submicron particles were produced with a hierarchical structure made of individual nanosized crystallites [24-25]. Unfortunately, this route suffers from many safety problems since supercritical alcohols are highly flammable and stringent security systems are therefore required in the reactor area.

For the sake of replacing organic solvents, other protocols were developed applying sub- and super-critical $CO_2$ as a reaction media for operating the hydrolysis and condensation of titanium tetra-isopropoxide ($Ti(O^iPr)_4$). Indeed, supercritical $CO_2$ (SC-$CO_2$) is an attractive, non-toxic, environmentally benign and low cost green solvent with

readily accessible critical point (Tc = 304.3 K, Pc = 7.38 MPa). It has been used as a solvent or anti-solvent in a large variety of materials processing and synthesis protocols [26] and it is particularly well adapted to the preparation of nanostructured materials [27-30]. Titanium alkoxides are reasonably soluble in SC-$CO_2$, and $Ti(O^iPr)_4$ exhibits the highest solubility among the commercially available compounds. This alkoxide thus enables easy formation of uniform $Ti(OH)_4$ particles when $Ti(O^iPr)_4$ is reacted with water in the SC-$CO_2$ reactor [31]. Thereafter several other authors published on the influence of the reaction pressure, temperature and molar ratio water/$Ti(O^iPr)_4$ on the characteristics of titania powders obtained under SC-$CO_2$ conditions [32-36]. A critical review summarizing the impact of these key-parameters and the basic principles of supercritical-based techniques applied to the production of nanostructured materials was published elsewhere [37]. In spite of large improvement in the synthesis protocols, several important process parameters are often neglected in the literature, and this might explain difficult up-scaling of the synthesis processes.

To shed further light into the key-parameters which have to be controlled for preparing $TiO_2$ anatase nanocrystalline powders, with the desire structure and microstructure in SC-$CO_2$, several strategies have been developed and compared by the authors. It must be noted that such synthesis approaches are nowadays of an utmost actuality as application of the supercritical fluids is attracting a constantly increasing interest of the scientific community. It is indeed recognized that this green and sustainable technology could become an alternative to many conventional synthesis techniques in organic solvents.

Hence, the present work is a detailed description of the results obtained in the framework of internal CEA research projects exploring the potential of supercritical fluids for preparing ceramic nanomaterials at large scale. Special emphasis was first devoted to controlling the effect of conventional processing parameters on powder characteristics, notably the role of the reaction temperature on the produced powders crystallinity degree, crystal phase, crystallite size, particle microstructure and specific surface area. In addition, other key process parameters such as SC-$CO_2$ pressure, stirring and water injection rate in the reactor were also investigated. Finally, the photocatalytic activity of the powders has been assessed, as a typical functional property of $TiO_2$ materials [38-45]. The performance of the nanocrystalline titania powders

prepared by the "green" SC-$CO_2$ process were compared with those of more conventional commercial $TiO_2$ powders.

## 2. Experimental section

Powders were prepared by reacting titanium tetraisopropoxide ($Ti(O^iPr)_4$) and water in supercritical $CO_2$, according to the conventional hydrolysis and condensation reactions pathway of sol-gel route (Eq. 1, 2 and 2'):

(Eq. 1) $$Ti(O^iPr)_4 + n\ H_2O \rightarrow Ti(O^iPr)_{4-n}(OH)_n + n\ {}^iPrOH$$

(Eq. 2) $$(O^iPr)_{4-n}(OH)_{n-1}Ti - OH + HO - Ti(O^iPr)_{4-n}(OH)_{n-1} \rightarrow (O^iPr)_{4-n}(OH)_{n-1}Ti - O - Ti\ (O^iPr)_{4-n}(OH)_{n-1} + H_2O$$

(Eq. 2') $$(O^iPr)_{4-n-1}(OH)_n\ Ti\ O^iPr + HO - Ti\ (O^iPr)_{4-n}(OH)_{n-1} \rightarrow (O^iPr)_{4-n-1}(OH)_n\ Ti - O - Ti\ (O^iPr)_{4-n}(OH)_{n-1} + {}^iPrOH$$

In the presence of water, the formation of hydroxyl groups is enhanced by very fast hydrolysis step in such a way that the condensation reaction between hydroxides (Eq. 2) is favoured, leading to hydroxide precipitation (Eq. 3):

(Eq. 3) $$Ti_NO_{2N-3-x/2}(OH)_{6+x} + (2N-3-x/2)\ H_2O$$

Crystalline $TiO_2$ can be obtained by increasing the temperature (Eq. 4), either by thermal post treatment of the hydroxide or directly *in situ*, by crystallization in supercritical $CO_2$.

(Eq. 4) $$Ti_NO_{2N-3-x/2}(OH)_{6+x} \xrightarrow{\Delta T} N\ TiO_2 + (3+x/2)\ H_2O$$

### 2.1. Chemicals

Chemicals and solvents were of analytical grade and used without any further purification. Titanium tetraisopropoxide ($Ti(O^iPr)_4$) (Fluka, 99 %) was selected as titanium precursor. Standard grade $CO_2$ ([$H_2O$] < 10 ppm) was supplied by Air Liquide. Pure water, with a resistivity of 18.2 MΩ, was produced by a Milli-Q system (Millipore USA). Commercial titania powder (Aeroxide® P25) was supplied by Evonik-Degussa. Methylene blue (MB) and Congo red (CR) dyes were purchased from Sigma Aldrich.

### 2.2. Experimental set-up and titania preparation protocol

Powders were synthesized in a lab scale device schematized in figure 1. The reaction was carried out either in a 500 ml or in a 1 litre high-pressure stirred vessel (Autoclave France). After introducing a specific amount of titanium alkoxide in the autoclave, liquid $CO_2$ was pumped into the vessel up to the operating pressure (10 - 30 MPa). An efficient mixing of the reactants was achieved with a magnetic turbine stirrer (stirring rate from 100 to 2000 rpm).

The reaction temperature was regulated from 323 K to 823 K using a thermocouple and an external electric heater. Water required for hydrolysis reaction was fed using a liquid chromatography pump with a flow ranging from 0.01 to 10 $ml.min^{-1}$. After the experiment, the pressure was released by evacuating $CO_2$ to the vent and a dry powder was recovered directly from the autoclave.

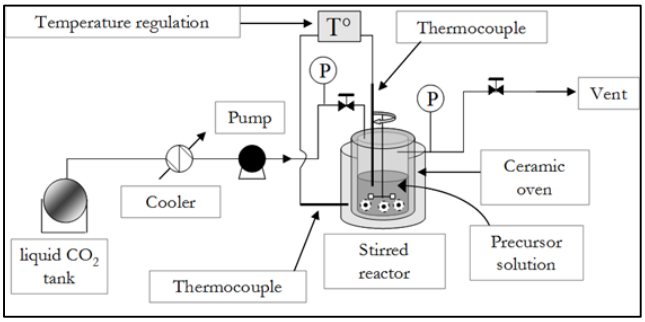


**Fig. 1** Experimental device used for titania powders synthesis in supercritical carbon dioxide

### 2.3. Characterisation methods

The morphology and microstructure of the synthesised powders were characterised by scanning electron microscopy (SEM – Cambridge Stereoscan 240) coupled with a secondary electron detector, $N_2$ adsorption-desorption (Micromeritics ASAP 2010) after powder outgassing at either 373 K for 12 h (amorphous powders) or 30 K below the synthesis temperature (crystalline samples). Small angle X-Ray scattering (Bruker AXS NanoStar) and infrared spectroscopy (FTIR- Nicolet Impact 400) were also used for completing powders analysis. The crystallisation of amorphous powders was studied *in situ* under secondary vacuum with a Siemens D500 X-ray diffractometer (XRD) from 313 K to 1023 K.

The thermal behaviour of the produced powders has been investigated by both TGA and TDA up to 1473 K (TA instrument system, 10 K/min in air flow). In addition, the sintering behaviour of $TiO_2$ powders (compacted at 8 tons.cm$^{-2}$ in a disc shape) has been investigated with a Setaram dilatometer, up to 1773 K in air.

The photocatalytic activity of the produced titania powders was evaluated by studying the degradation of Methylene Blue and Congo Red dyes (model pollutants) in water.

In order to eliminate possible impurities (e.g. unreacted precursors, carbonaceous residues) which might influence the photocatalytic efficiency of $TiO_2$ powders, the samples were first washed in isopropanol under sonication for 10 min, rinsed with water and dried 24 h at 80°C.

For all experiments, titania powder suspensions (0.2 g.L$^{-1}$) were prepared in deionized water and sonicated during 10 min. The surface charge (zeta potential) and size of the aggregates obtained in aqueous suspensions (Dynamic Light Scattering – DLS) were measured with the help of a Zetasizer (Malvern).

For each photocatalytic test, 100 ml of the aqueous suspension were mixed with 100 ml of dye solution (10 mg.L$^{-1}$). The as-prepared suspensions were stirred for 5 minutes in a dark chamber and then submitted to UV irradiations ($\lambda$ = 365 nm) up to 30 h. Samples (5ml) were regularly withdrawn from the mother solution and filtered before characterization by UV/vis spectroscopy (Lambda 40 Perkin Elmer).

## 3. Results and discussion

Two strategies have been studied in this work to prepare $TiO_2$ nanopowders under supercritical conditions. The first strategy bears on the preparation of an amorphous $Ti(OH)_4$ powder which was subsequently crystallized by post-thermal treatment, while the second one is based on the direct formation of crystalline $TiO_2$ (anatase) in SC-$CO_2$. The key characteristics of both synthesis protocols have been examined by varying the processing parameters and studying their influence on the final powder characteristics in relation with their morphology, microstructure, crystallinity, thermal behaviour and photocatalytic activity for the degradation of model pollutants in water media.

### 3.1. Amorphous $Ti(OH)_4$ powders synthesized in SC-$CO_2$

*Reactant solubility and operating parameters*

In a first step, hydrolysis and condensation of titanium tetraisopropoxide ($Ti(O^iPr)_4$) was studied at low temperature under supercritical conditions (30 MPa - 323 K). In order to determine the appropriate amounts of reactants to be introduced into the reactor, the solubility data for both $Ti(O^iPr)_4$ and water in SC-$CO_2$ were evaluated.

The extraction yield of the alkoxide by SC-$CO_2$ was measured in the aforementioned standard operating conditions and was determined to be ~4.5 wt% (a value of 4.25 wt% was reported in the literature in slightly different operating conditions [31]). The alkoxide concentration in the reactor was consequently fixed at ~4 wt% in order to ensure a single phase reaction.

Because of the non-polar character of $CO_2$, water solubility in SC-$CO_2$ is known to be very low (typically 0.2 wt%). A low water injection flow rate ~10 ml/min was thus applied in the first series of experiments and pressure was released immediately after water injection to maintain a constant pressure (30 MPa). The above selected flow rate was five times lower than the maximum value allowed by water solubility (0.2 wt%) under the selected experimental conditions [46].

The involved chemical reaction is given below (Eq 5):

(Eq. 5) $$Ti(OiPr)_4 + 4\,H_2O \xrightarrow[SC-CO_2]{30\ MPa-323\ K} Ti(OH)_4 + 4\,iPrOH$$

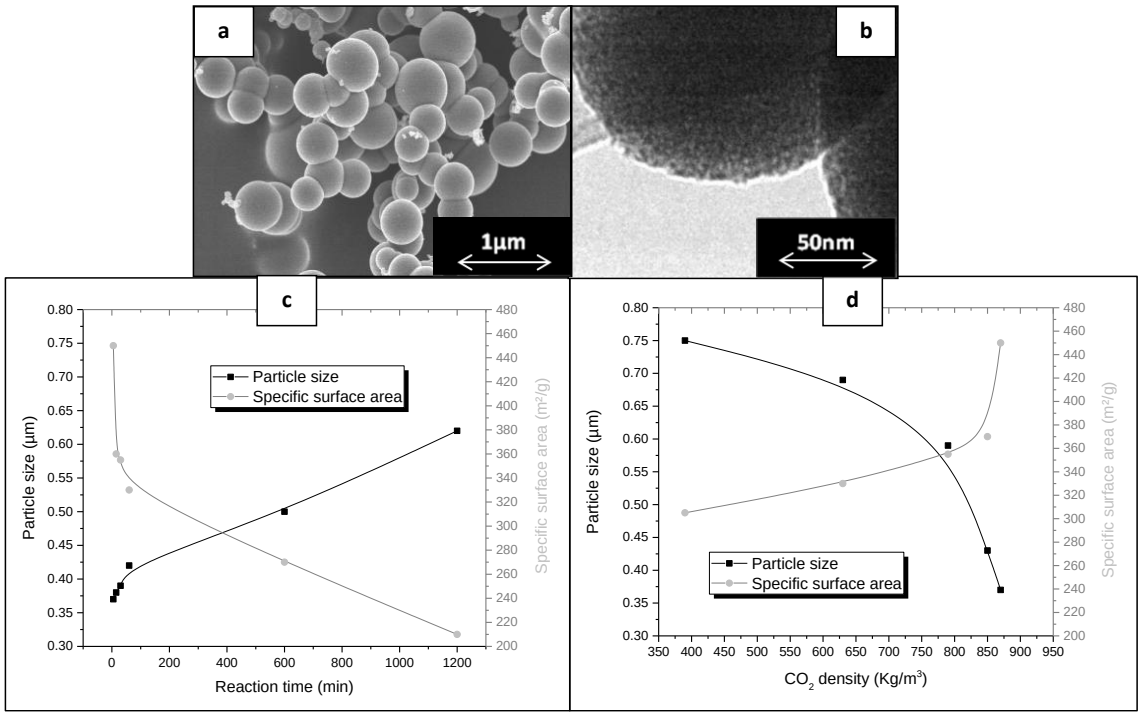


**Fig. 2** Microstructural characteristics of amorphous $Ti(OH)_4$ powders obtained by reacting $Ti(O^iPr)_4$ with $H_2O$ in SC-$CO_2$ at 323 K and 30 MPa: a) SEM observation, b) TEM observations, c) Evolution of mean particle sizes and $S_{BET}$ as a function of reaction time/maturation in SC-$CO_2$ and d) as a function of SC-$CO_2$ density. (Stirring rate: 1000 rpm, water injection rate: 10 ml.min$^{-1}$)

Both the unreacted alkoxide and formed isopropyl alcohol (both soluble in SC-$CO_2$) were easily separated from the prepared hydroxide, during pressure release. The standard conditions (30 MPa - 323 K) led to the production of an amorphous powder corresponding to submicron-sized spherical particles (Figure 2a).

No significant variation of the average particle sizes was observed when changing the alkoxide concentration while keeping the hydrolysis ratio constant. In other respect, when the alkoxide concentration was set at 4 wt% and the hydrolysis ratio was less than 4 (stoichiometry for complete hydrolysis of the $Ti(O^iPr)_4$ alkoxide), the average size of particles was found to slightly decrease from 0.37 to 0.30 µm, but this variation was not considered as significant.

*Characteristics of amorphous SC-$Ti(OH)_4$ powders (323 K, 30 MPa, $H_2O$: 10 ml/min)*

As a consequence of high reactivity of the titanium alkoxide, large surface area and fluffy hydroxide powders were directly obtained in the reactor. No carbonate species

were detected in the powders by FTIR spectroscopy, despite of using water in $CO_2$ medium. In order to calculate the synthesis yield, the amorphous powder has been submitted to a 12 h thermal treatment at 1273 K in air. A molar yield around 70% has been calculated by considering the amount of $TiO_2$ expected from the fed quantity of TTIP precursor. As expected at such low reaction temperature (323 K), TTIP was partially unreacted and residual precursor was vented with $CO_2$ at the end of the experiment.

SEM and TEM observations (Figure 2a & 2b, respectively) revealed a hierarchical structure of the synthesized powders. The spherical particles, relatively uniform in size (diameters in the range 0.15 - 0.5 µm), were partially agglomerated (Figure 2a). Each of them consisted of a compact stacking of titanium hydroxide nanoparticles (Figure 2b).

The apparent density measured for the as-prepared powder was 0.24 whereas the intrinsic density measured by helium pycnometry (Quantachrom system) was 2.80, thus suggesting large pore volumes between and within the spherical particles. The $N_2$ adsorption-desorption isotherms measured for the powders dried at 373 K for 12 h, was mainly of type I, i.e. typical for a microporous material (results not shown). The total pore volume was 0.22 $cm^3.g^{-1}$ with 80 % microporosity and the BET specific surface area was 450 $m^2.g^{-1}$. It is interesting to note that a higher value of specific surface area (750 $m^2.g^{-1}$) was measured for the same sample when applying a non-intrusive method such as Small Angle X-ray Scattering. The SAXS technique is sensitive to surface rugosity and is able to detect pores which are not accessible to $N_2$ molecules (closed pores and ultramicropores). This technique also confirmed that the spheres were composed of nanometer-sized aggregated primary particles.

*Influence of reaction time and $CO_2$ density on powder characteristics*

One of the advantages arising from the application of supercritical fluids bears on the possibility of adjusting the solvent pressure and thus its density (impacting on solutes diffusion rate) while maintaining a single phase medium. In the aforementioned reaction conditions, the characteristics of the produced powders could be affected by two key parameters: i) reaction time after water injection and ii) pressure of the $CO_2$ phase. The influence of both parameters on particle sizes and specific surface areas of the titanium hydroxide powders are reported on table 1. The evolution of mean particle sizes and

specific surface areas versus reaction time and SC-$CO_2$ density is plotted in figures 2c and 2d, respectively.

**Table 1:** Characteristics of $Ti(OH)_4$ powders prepared in SC-$CO_2$ at 323 K at different synthesis pressures and reaction times (stirring rate: 1000 rpm, water injection rate: 10 $ml.min^{-1}$)

| **Pressure (MPa)** | **$CO_2$ density ($kg.m^{-3}$)** | **Reaction Time (min)** | **Particle size (µm)** | **$S_{BET}$ ($m^2.g^{-1}$)** |
|---|---|---|---|---|
| 30 | 870 | 5 | 0.37 | 450 |
| 30 | 870 | 15 | 0.38 | 360 |
| 30 | 870 | 30 | 0.39 | 355 |
| 30 | 870 | 60 | 0.42 | 330 |
| 30 | 870 | 600 | 0.50 | 270 |
| 30 | 870 | 1200 | 0.62 | 210 |
| 27 | 850 | 5 | 0.43 | 370 |
| 20 | 790 | 5 | 0.59 | 355 |
| 13 | 630 | 5 | 0.69 | 330 |
| 10 | 390 | 5 | 0.75 | 305 |

The observed increase in particle sizes with the reaction time suggests a growing mechanism comparable to the Ostwald ripening in suspensions where the smallest particles coalesce to feed the larger ones [47]. Concurrently, both the specific surface area and microporous volume fraction decrease when the reaction time increases. On the other hand the total pore volume and mean pore sizes increase. For a reaction time of 20 h, a mesoporous powder was obtained (type IV -$N_2$ adsorption/desorption isotherms) with a total pore volume of 0.36 $cm^3.g^{-1}$.

When decreasing the system pressure from 30 MPa down to 10 MPa, the average particle sizes increased by a factor x2. This was attributed to the increasing diffusion coefficient of solutes when the SC-$CO_2$ density decreases. Consequently, lower working pressures statistically increase the number of interactions between titanium hydroxide nanoparticles, favoring their aggregation and therefore increasing the average size of the final particles.

In conclusion, powders with very high specific surface area (~450 $m^2/g$) and small cluster sizes (~ 1 nm) were obtained for amorphous titanium hydroxides synthesized in SC-$CO_2$ at low temperatures (< 473K). Small nuclei were obtained as a result of SC-

$CO_2$ specific properties such as low viscosity and high density, enabling fast reaction kinetics. Hence, clusters tend to condense at low temperatures in very short reaction time. In addition, cluster growth is also limited due to pressurized media, low $CO_2$ surface tension and $CO_2$ sorption on hydroxide surface.

### 3.2 Conversion of amorphous $Ti(OH)_4$ powders to crystalline $TiO_2$ powders by thermal post-treatment

For the sake of obtaining crystalline $TiO_2$ particles, a thermal post-treatment was conducted with the as-prepared amorphous titanium hydroxide powders. XRD analysis under vacuum revealed that the amorphous powder transformed to anatase crystalline phase between 613 and 633 K. The rutile phase transition was found to occur between 1023 and 1123 K. These results (not shown) fit the data reported in [48] for microsized $TiO_2$ particles. During the thermal treatment, the powder surface area decreased from 450 $m^2.g^{-1}$ at 373 K, down to 5 $m^2.g^{-1}$ at 813 K (Table 2). The anatase powder obtained at 813 K was found to be mainly macroporous/non porous (Type III- $N_2$ adsorption/desorption isotherms). On the other hand, the thermal treatment changed very slightly the powder morphology: spherical particles were obtained with a slightly smaller diameter (typically around 460 μm at 813 K).

**Table 2:** Influence of thermal post-treatment temperature (1 h) on the characteristics of $Ti(OH)_4$ powders prepared in SC-$CO_2$ at 323 K and 30 MPa

| Post-treatment temperature (K) | Particle size (μm) | $S_{BET}$ ($m^2.g^{-1}$) | Cristalline phase | Porous structure |
|---|---|---|---|---|
| No | 0.37 | 450 | Amorphous | Microporous |
| 453 | 0.42 | 445 | Amorphous | Microporous |
| 523 | 0.43 | 105 | Amorphous | Mesoporous |
| 633 | 0.40 | 5 | Anatase | Macroporous / non porous |
| 813 | 0.46 | 5 | Anatase | Macroporous / non porous |
| 993 | 0.43 | 3 | Anatase | Macroporous / non porous |

In order to further investigate the characteristics of the $TiO_2$ powders obtained by thermal post-treatment of SC-$CO_2$ $Ti(OH)_4$ particles, a series of pellets have been prepared (compacted at 8 tons/cm$^2$) and studied by dilatometry up to 1773 K.

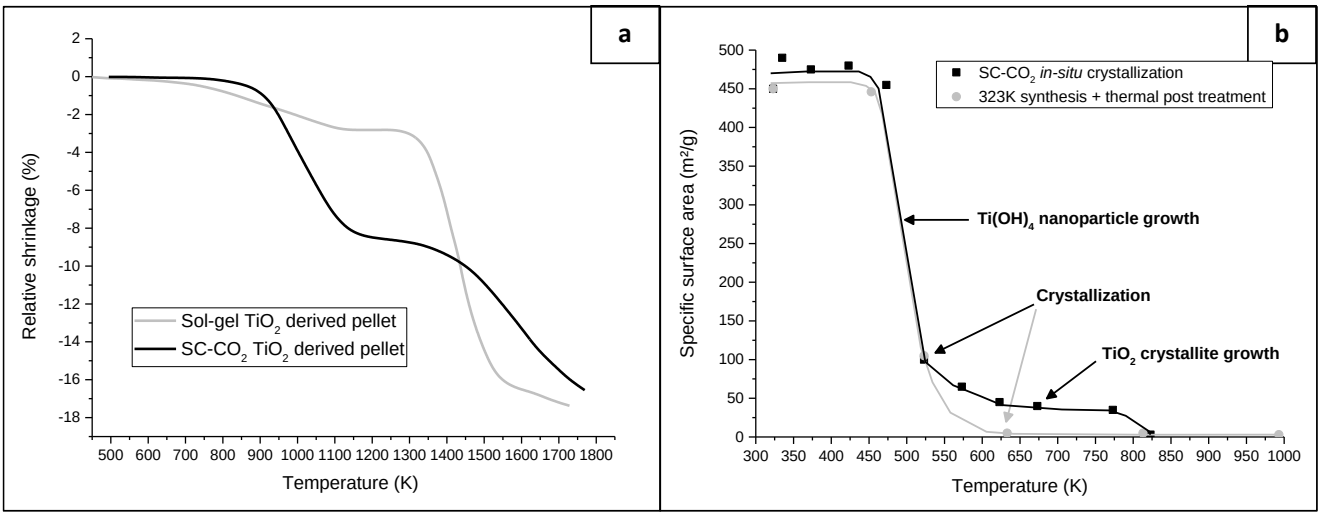


**Fig. 3** Thermal evolution of titania powders: a) Comparison of sintering behavior of a powder prepared in SC-$CO_2$ at 323 K, 30 MPa and a sol-gel derived powder (discs with green density ~ 50 %), b) Specific surface area vs. synthesis temperature in SC-$CO_2$ (*in situ* crystallization) and specific surface area vs. post-treatment temperature of an amorphous powder prepared at 323 K, 30 MPa in SC-$CO_2$

The sintering behavior of pellets made from titania powder prepared by post-treatment at 723 K of SC-$CO_2$ $Ti(OH)_4$ formed at 323 K, has been compared with that of pellets made from a classical sol-gel derived powder prepared under atmospheric conditions. This latter consisted of aggregated nanosized particles of 8 nm in size. Starting from a green relative density of about 50 % for both pellets, the SC-$CO_2$ and classical sol-gel derived samples both reached a relative density of 97 - 99 % at 1723 K. As shown in figure 3a, and contrary to the classical sol-gel sample, the SC-$CO_2$ sample clearly displayed two-steps densification process.

The first one, between 873 K and 1073 K, has been attributed to pore volume collapse inside spherical particles (intra-particle sintering). Due to this phenomenon, a relative density of about 75 % is obtained at 1100 K for the SC-$CO_2$ pellet, compared to only 60 % for the classical sol-gel pellet. A second densification step is observed for the SC-

$CO_2$ pellet: it starts at ~1473 K and corresponds to a sintering between individual particles (inter-particles sintering). For sol-gel derived powders, a more conventional sintering process is observed: pellet densification starts at temperature around 1323 K and it is almost completed at 1700 K. Densification of the SC-$CO_2$ pellets could be facilitated by using a pressure-assisted sintering process, able to compact the individual particles during/after the intra-particle sintering step, as already demonstrated by our research group for zirconia powder prepared in SC-$CO_2$ [49-50].

### 3.3. Direct synthesis of nanocrystalline $TiO_2$ anatase powder in SC-$CO_2$

In previous works, the authors synthesized crystalline zirconia from metal-organic precursors in SC-$CO_2$ by applying high synthesis temperatures directly in the reactor [50-53]. Zirconia crystallisation was attained under supercritical conditions at lower temperatures compared to conventional sol-gel and thermal treatment protocols. In the present work, direct synthesis of crystalline $TiO_2$ ultra-fine particles has been performed in SC-$CO_2$ at 30 MPa and in the temperature range 323 - 823 K. In order to modify the reaction kinetics and better control particle formation, two hydrodynamic key-parameters: water injection and stirring rates, have been investigated in addition to the reaction temperature. The influence of these parameters on the derived $TiO_2$ powder characteristics is discussed hereafter.

*Influence of reaction temperature on $TiO_2$ powders structure and microstructure*

Direct synthesis of $TiO_2$ anatase powders in the reactor under supercritical conditions and mild synthesis temperatures revealed much more effective than hydroxide thermal post-treatment for obtaining uniform crystalline nanoparticles with high specific surface area. The anatase structure was detected by XRD already for synthesis temperature of 523 K whereas, in conventional thermal treatment at atmospheric pressure, titanium hydroxide was found to crystallize to anatase only at 613 K. Results reported on table 3 clearly demonstrate that anatase $TiO_2$ can be obtained under supercritical conditions between 523 and 823 K. It is also worth noting that the amorphous $Ti(OH)_4$ powder obtained at 423 K can be easily converted to anatase by a post-treatment at 573 K while maintaining a large specific surface area of 190 $m^2.g^{-1}$ (Table 3). This finding suggests that the crystallization process starts already below 523 K although it cannot be detected with XRD (too small crystallites).

Table 3: Characteristics of $TiO_2$ powders prepared in SC-$CO_2$ within 5 min reaction time at 30 MPa in the temperature range 323 – 823 K (stirring rate: 1000 rpm, water injection rate: 10 $ml.min^{-1}$).

| **Sample reference (#)** | **Synthesis conditions** | | **Powder characteristics** | | | |
|---|---|---|---|---|---|---|
| | **Synthesis temperature (K)** | **$CO_2$ density ($kg.m^{-3}$)** | **$S_{BET}$ ($m^2.g^{-1}$)** | **Crystalline phase** | **Color** | **Porous structure** |
| 1 | 323 | 870 | 450 | Amorphous | White | Microporous |
| 2 | 373 | 660 | 475 | | | |
| 3 | 423 | 490 | 480 | | | |
| 3.1 | Sample #3+ thermal post treatment at 573 K – 3 h | | 190 | Anatase | | Mesoporous |
| 4 | 473 | 390 | 455 | Amorphous | | Microporous |
| 5 | 523 | 330 | 100 | Anatase | Beige | Mesoporous |
| 6 | 573 | 280 | 65 | | | |
| 6.1 | Sample #6 + thermal post-treatment at 573 K – 1 h | | 75 | | White | |
| 6.2 | Sample #6 + thermal post-treatment at 873 K – 3 h | | 30 | | | |
| 6.3 | Sample #6 + thermal post-treatment at 1073 K – 3 h | | 1 | 80% Rutile 20% Anatase | White | Non porous |
| 7 | 623 | 250 | 45 | Anatase | Beige | Mesoporous |
| 8 | 673 | 230 | 40 | | Light Brown | |
| 9 | 773 | 200 | 35 | | Dark Brown | |
| 9.1 | Sample #9 + thermal post-treatment at 773 K – 1 h | | 45 | | White | |
| 10 | 823 | 180 | 3 | | Black | Non porous |
| 10.1 | Sample #10 + thermal post-treatment at 823 K – 3 h | | 20 | | White | Mesoporous |

The lower crystallization temperature observed in SC-$CO_2$ is attributed to the positive effect of solvothermal conditions on the oxide formation, due to the energy conveyed by the pressure in the supercritical phase. Interestingly, the hierarchical structure of amorphous $Ti(OH)_4$ particles is maintained after crystallization. The anatase powders directly formed in SC-$CO_2$ are mesoporous and their specific surface varies in the range 20 - 100 $m^2.g^{-1}$ depending on the synthesis temperature (Figure 3b). For comparison, the powders obtained by thermal post-treatment of $Ti(OH)_4$ in air at 613 K, are macroporous/non porous with a low specific surface area of about 5 $m^2.g^{-1}$ (Figure 3b).

The morphologies of particles obtained at different synthesis temperatures are compared in figure 4. No significant influence of the temperature was observed below 523 K: spherical polydispersed particles (~ 0.5 µm in diameter) were obtained and their specific surface area was maintained in the range 400-500 $m^2.g^{-1}$ up to the crystallization temperature. At higher temperatures (523 – 823 K) the decrease of SC-$CO_2$ density and associated increase of self-diffusion coefficients for nanoparticles and/or reacting species led to a modification of crystalline particles morphology. Indeed, powder characteristics drastically change at temperatures above 523 K, which corresponds to the crystallization temperature. Under these experimental conditions, particles become smaller (Ø = 0.2 µm), monodispersed and mesoporous. This structure change reflects the formation of primary crystalline $TiO_2$ particles which are larger than the initial $Ti(OH)_4$ ones.

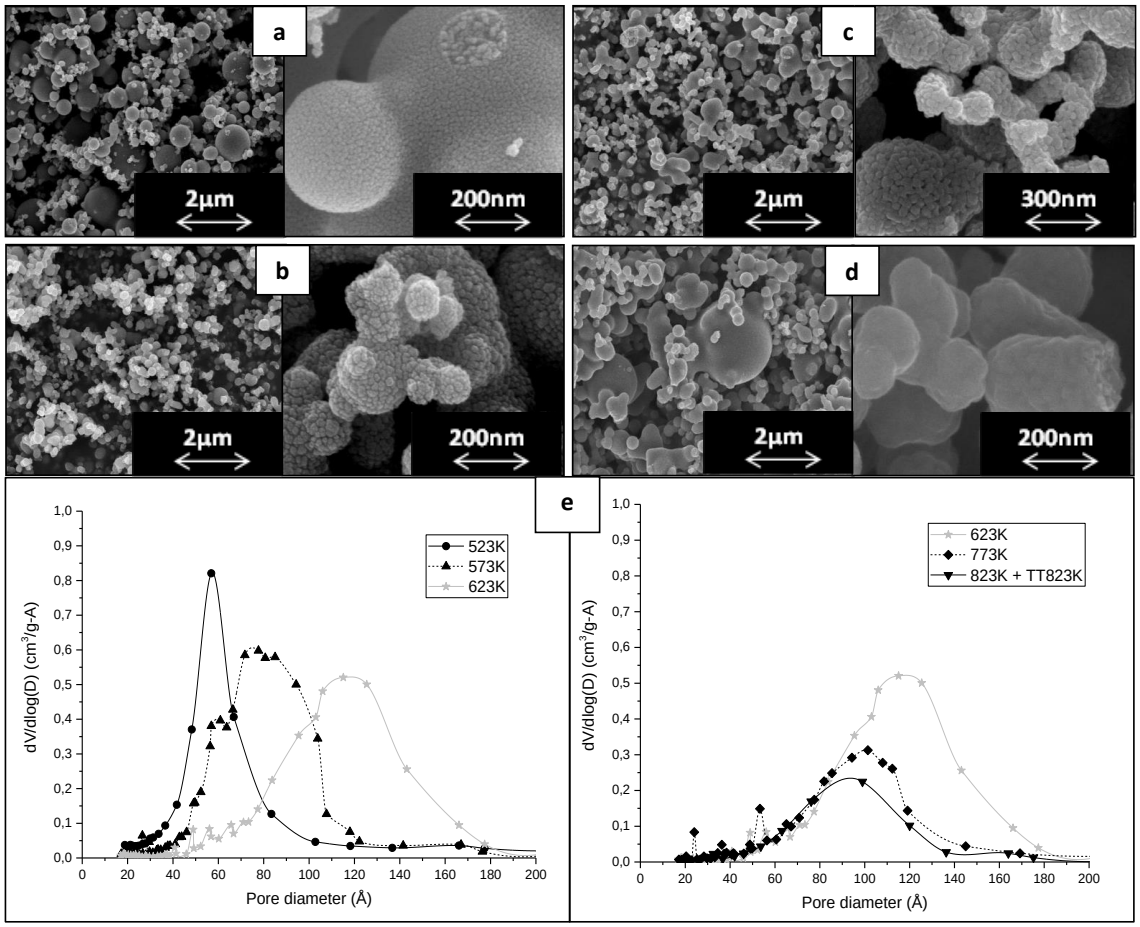


**Fig. 4** Evolution of $TiO_2$ particles morphology and pore size distribution (PSD) as a function of the synthesis temperature at 30 MPa in SC-$CO_2$: SEM images of powders

prepared at a) 423 K, b) 573 K, c) 773 K, d) 823 K. PSD of powders synthesized at 523 K, 573 K, 623 K, 773 K, and 823 K are compared in e). (Stirring rate: 1000 rpm, water injection rate: 10 $ml.min^{-1}$)

The size of primary crystallites estimated from both XRD line width and $S_{BET}$ values are reported in Table 4 for $TiO_2$ powders obtained between 523 and 823 K.
As expected, when the synthesis temperature was increased, crystallite sizes increased and both specific surface areas and pore volumes decreased. Remarkably, brown and dark powders were obtained above 573 K (Figure 5c). This colour was attributed to carbon residues resulting from the thermal decomposition of the titanium alkoxide organic chain, released during the hydrolysis and condensation reaction. Indeed, white powders could be recovered after a thermal post-treatment in air above 573 K.

**Table 4:** Comparison of pore volume, crystallite sizes, TGA weight loss and synthesis yields for $TiO_2$ powders prepared in SC-$CO_2$ at 30 MPa within 5 min reaction time in the temperature range 523 – 823 K

| **Sample reference (#)** | **Synthesis temperature (K)** | **Synthesis yield (%)** | **Pore volume ($cm^3.g^{-1}$)** | **Pore size (nm)** | **$\varnothing_{crystallites}$ from DRX (nm)** | **$\varnothing_{crystallites}$ from $S_{BET}$ (nm)** | **Weight loss at 823K (%)** |
|---|---|---|---|---|---|---|---|
| 5 | 523 | 94 | 0.20 | 4.8 | 16 | 17 | 8 |
| 7 | 623 | 77 | 0.15 | 11.7 | 24 | 35 | 3 |
| 9 | 773 | 65 | 0.10 | 10.2 | 24 | 43 | 9 |
| 10 | 823 | 71 | - | - | 27 | 513 | 24 |
| 10.1 | Sample#10 + TT823K-3h | - | 0.07 | 9.2 | 40 | 73 | 1 |

Accordingly, TGA & DSC analysis (Figure 5a & 5b, respectively) clearly demonstrated the existence of carbonaceous residues and their decomposition upon heating. Comparison of TGA mass losses for powders prepared at different temperatures in SC-$CO_2$ (Table 4) revealed the formation of a higher quantity of carbon for the highest synthesis temperatures. In fact, significant quantities of carbon were detected for synthesis temperatures ≥ 773 K. At 823 K, the quantity of carbon was abundant (24 % mass loss) and resulted in a very low specific surface area (3 $m^2.g^{-1}$) caused by pore clogging, as shown in figure 5d.

The carbonaceous film covering the titania spherical particles can be easily eliminated by a simple thermal post-treatment in air at 823 K. In fact, the pores and internal surface of the derived white powder become accessible to $N_2$ and $S_{BET}$ values increased from 3 to 20 $m^2.g^{-1}$ after thermal oxidation of carbon species. Indeed, similar pores blocking phenomenon by carbonaceous residues, resulting in powders with lower specific surface areas, has been also evidenced for samples prepared at 573 and 773 K (Table 3).

Another indication/consequence of carbon species formation is the increasing discrepancy between crystallite sizes calculated from $S_{BET}$ values and XRD lines analysis (Table 4) when synthesis temperature was increased. In addition, the synthesis yield (calculated from expected $TiO_2$ amount and taking into account the TGA weight loss measured at 823 K) was almost 94 % at 573 K but drastically decreased when the synthesis temperature was increased.

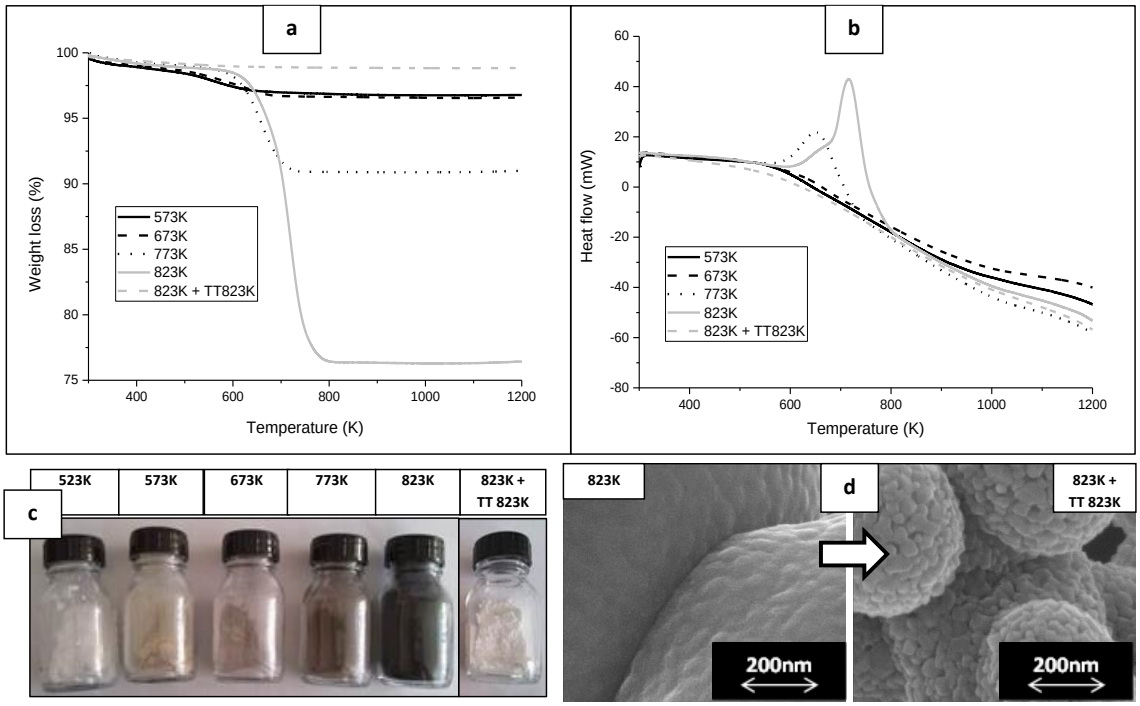


**Fig. 5** Evidence of residual carbonaceous species in $TiO_2$ powders prepared in SC-$CO_2$ at 30 MPa: a) TGA, b) DSC analysis; c) powders prepared at different temperatures in the range 523K-823K; d) SEM image of $TiO_2$ powder prepared at 823 K, before and after an additional post-treatment of 3 h in air at 823 K

In order to study the thermal stability of a $TiO_2$ powder prepared in SC-$CO_2$ at 573 K, samples were treated for 3h in air at 873 and 1073 K, and analysed by $N_2$ physisorption, XRD and SEM. The evolution of particle microstructure is shown in figure 6b. In comparison with the bare powder, the post-treatment at 873 K resulted in individual crystallite growth and simultaneous decrease of specific surface area (30 $m^2/g$ instead of 65 $m^2.g^{-1}$ initially). However, it must be noted that particle microstructure was still preserved at this temperature. When the starting powder was treated at 1023 K, intra-particle sintering occurred, yielding denser spherical particles and a dramatic decrease of their specific surface area (1 $m^2.g^{-1}$ instead of 65 $m^2.g^{-1}$ initially). In fact, the internal densification of individual particles also corresponds to the progressive transformation of anatase to rutile phase, as revealed by XRD (Figure 6a).

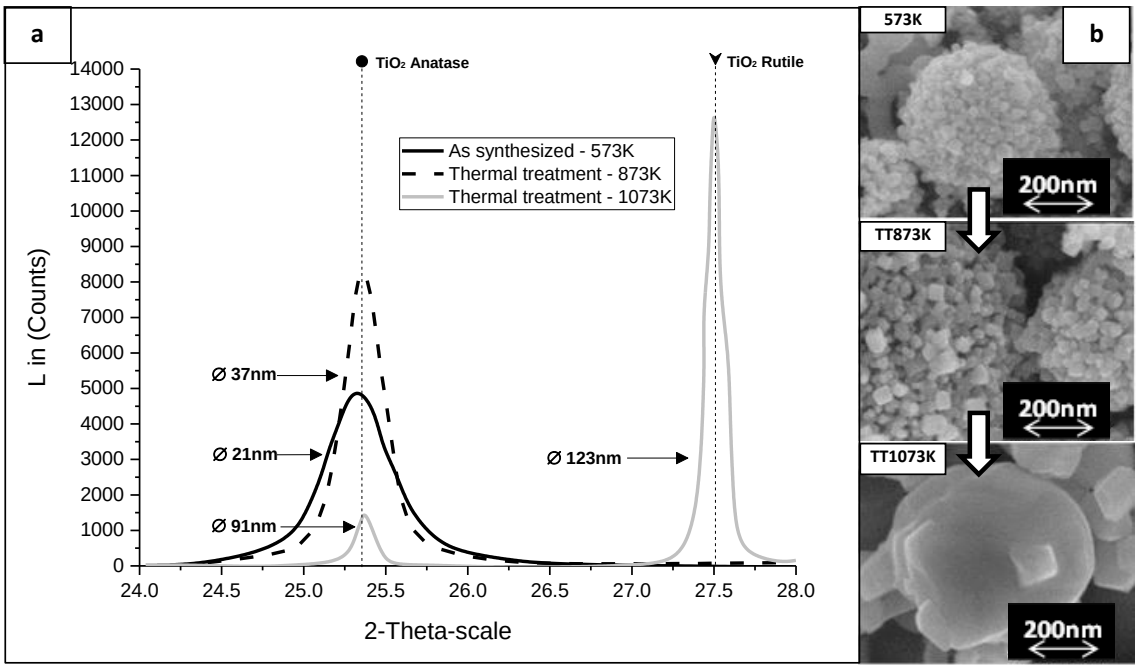


**Fig. 6** Thermal evolution (in air) of a $TiO_2$ powder prepared in SC-$CO_2$ at 573 K and 30 MPa, and post-treated for 3 h in air at 873 K and 1073 K: a) XRD patterns of powders with calculated crystallite sizes and b) SEM images of particles microstructure, with associated $S_{BET}$ values. (Stirring rate: 1000 rpm, water injection rate: 10 $ml.min^{-1}$)

*Influence of hydrodynamic parameters on particle morphology and aggregation*

In the supercritical process used in this work for the synthesis of crystalline $TiO_2$ powders, both water injection rate and steering rate are key-parameters with a direct impact on powder morphology and specific surface area. Various combinations of these parameters were tested, as reported in table 5. The quantity of injected water was fixed to 4 moles $H_2O$ for 1 mole of titanium alkoxide. The temperature and pressure of the SC-$CO_2$ phase were set at 523 K and 30 MPa, respectively.

**Table 5:** Influence of hydrodynamic parameters (water injection and stirring rates) on the specific surface area of $TiO_2$ powders prepared in SC-$CO_2$ at 30 MPa within 5 min reaction time at 523 K

| **Water injection rate ($ml.min^{-1}$)** | **Stirring rate (rpm)** | **$S_{BET}$ ($m^2.g^{-1}$)** |
|---|---|---|
| 1 | 700 | 100 |
| 1 | 1000 | 130 |
| 5 | 700 | 105 |
| 10 | 300 | 95 |
| 10 | 700 | 90 |
| 10 | 1000 | 100 |
| 10 | 2000 | 110 |

As mentioned above, both hydrolysis and condensation reactions of $Ti(O^iPr)_4$ alkoxide are involved in $Ti(OH)_4$ clusters formation and thus impact on the formation of $TiO_2$ primary particles. The as-formed primary particles diffuse and collide in the supercritical phase, yielding secondary spherical particles. Considering the fact that hydrolysis of alkoxy groups is a very fast reaction in presence of a stoichiometric quantity of water, the formation of spherical secondary particles can be described as a diffusion-limited process. This is the case when the water injection rate is 10 ml/min. On the contrary, for lower water injection rates (1 $ml.min^{-1}$) it can be assumed that alkoxide hydrolysis is not fully completed before the formation of spherical particles. It can be thus ascribed to a reaction limited process. The effect of water injection rate on particle morphology can be clearly observed in figure 7. For a water injection rate ~ 1 $ml.min^{-1}$, small particles were obtained with narrow size distribution but irregular geometry. This finding results from the coincidence of clusters and particles formation in a reaction limited process. For higher water injection rate (~ 10 $ml.min^{-1}$) and comparable stirring rate (700 rpm), powder specific surface areas were similar (90 - 100

$m^2.g^{-1}$) but particles had a better defined spherical geometry. This, results from the fact that complete hydrolysis and cluster formation take place before the formation of spherical particles.

The second hydrodynamic parameter investigated in this study was the stirring rate. The specific surface areas of powders prepared at 523 K with gradually increasing the stirring rate (from 300 to 2000 rpm) are compared in table 5. The $S_{BET}$ values were found to increase insignificantly with the stirring rate (e.g. from 90 to 110 $m^2.g^{-1}$ with 10 $ml.min^{-1}$ water injection rate). On the other hand, the stirring rate was found to strongly influence powders morphology as shown in figure 7. Large aggregates with undefined geometries were generally observed at high stirring rates. As shown in table 5, the highest value of the specific surface area (130 $m^2.g^{-1}$) was obtained when combining a medium stirring rate (~ 1000 rpm) and a low water injection (~ 1 ml/min). The results obtained in this paragraph demonstrate the strong impact of hydrodynamic parameters on the quality and homogeneity of the formed powders.

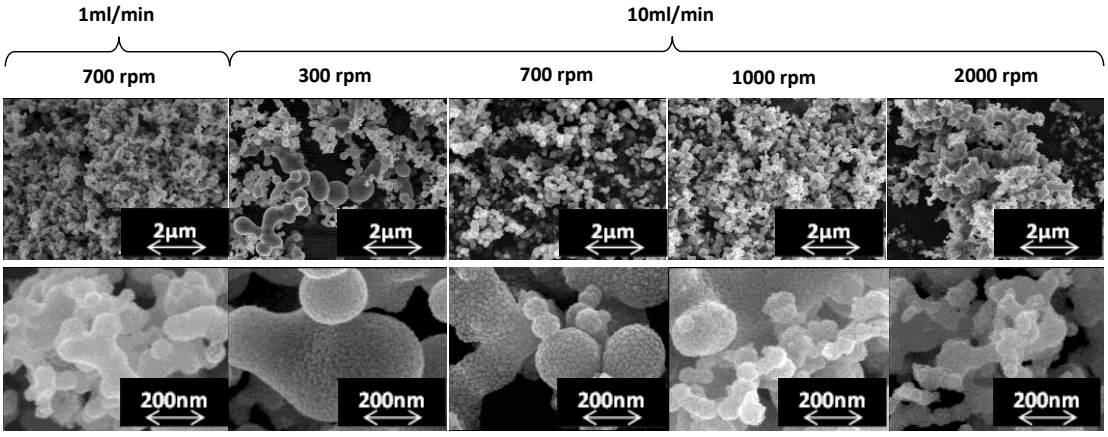


**Fig. 7** Influence of hydrodynamic parameters: water injection rate and stirring rates, on the morphology of $TiO_2$ particles prepared in SC-$CO_2$ at 523 K and 30 MPa, within 5 minutes reaction time

It is of utmost importance to note that the optimized operating parameters assessed in this work enabled also an up-scaled production of $Ti(OH)_4$ (373 K – 20 MPa) or anatase $TiO_2$ (573 K – 30 MPa) powders (70-80g in one single batch) when carrying out the synthesis in a large scale reactor facility described elsewhere [50]. Hence, high quantities of titania powders with similar characteristics to their lab-scale analogues

have been obtained, exhibiting controlled morphology (spherical particles from 0.1 to 0.8 µm in diameter), structure (amorphous or crystalline powders composed of < 15 nm primary particles) and microstructure (pore volume around 0.30 $cm^3.g^{-1}$; $S_{BET}$ of about 540 $m^2.g^{-1}$ for $Ti(OH)_4$ and 112 $m^2.g^{-1}$ for anatase $TiO_2$).

### 3.4. Photocatalytic activity: a functional property of $TiO_2$ anatase powders

The photocatalytic properties of $TiO_2$ anatase powders are classically evaluated by testing the degradation of model compounds in water media. Indeed, water decontamination with $TiO_2$ photocatalysts principally requires a high specific surface area of the photoactive material and UV light from either solar or artificial light sources [54]. Many water treatment applications have been already demonstrated with $TiO_2$ based materials, such as disinfection, remediation of metal contamination, oxidation of arsenite or removal of volatile organic compounds (VOC) [55]. The AEROXIDE® $TiO_2$ powder P25 (Evonik-Degussa) is usually considered as a reference highly active photo-catalyst. It was thus used in the present work to compare the performance of two $TiO_2$ powders prepared in SC-$CO_2$ at 30 MPa: an amorphous powder prepared at 423 K (#$Ti(OH)_4$ - 423 K) and a crystalline anatase powder prepared at 573 K (#$TiO_2$ – 573 K).

*Titania powder behavior in aqueous suspensions*

Since photo-catalytic treatment of liquid effluents takes place in aqueous solutions and photo-catalysis is a surface-dependent mechanism, it was important to investigate/compare first the behavior of $TiO_2$ powders in suspensions. Actually, particle aggregation as well as surface charges and surface chemistry might vary depending principally on the effluent pH.

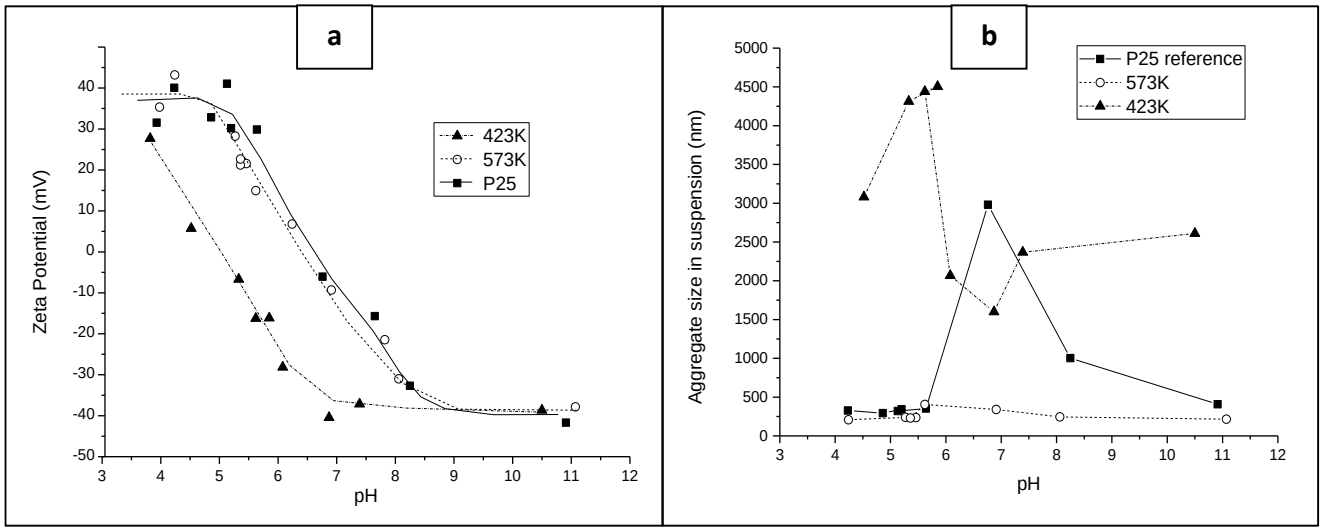


**Fig. 8** Influence of pH on the characteristics of suspensions prepared by dispersing the powders in water $Ti(OH)_4$ - 423 K and $TiO_2$ - 573 K prepared in SC-$CO_2$ and a commercial $TiO_2$ - P25 powder: a) Zeta potential and b) size of aggregates (by DLS) versus pH

Suspensions were prepared by dispensing the selected $TiO_2$ powders in water (concentration 0.2 $g.L^{-1}$). Both the zeta potential and size of aggregates (DLS) were determined. As observed in figure 8a, similar zeta potential trends were found for both crystalline powders (#$TiO_2$ - 573 K and #$TiO_2$ - P25), with an isoelectric point between pH = 6 and 7. However, a more acidic isoeletric point at pH = 5 was found for the amorphous powder #$Ti(OH)_4$ – 423 K. The evolution of aggregates sizes versus pH is drawn in figure 8b. The size distribution of aggregates for each sample is logically centered at the pH value corresponding to the isoelectric point. The amorphous powder #$Ti(OH)_4$ – 423 K displayed the largest aggregates in aqueous suspension. When comparing the two crystalline powders, larger aggregates were measured for #$TiO_2$ - P25 when pH ≥ 6, although comparable aggregates sizes were measured in both samples for pH < 6.

Each powder suspension has been then mixed with the same volume of a methylene blue solution (concentration MB 10 $mg.L^{-1}$, pH = 6.3), chosen as a model compounds for the photodegradation tests. The suspensions characteristics (zeta potential and sizes of aggregates) are reported on table 6. In terms of aggregate sizes and surface accessible to UV, both crystalline samples (#$TiO_2$ – 573 K and #$TiO_2$ - P25) were quasi-equivalent.

In comparison, the amorphous sample contains significantly larger aggregates and thus 10 times lower accessible surface for UV irradiation.

**Table 6:** Characteristics of $TiO_2$ powders used in aqueous suspensions for the degradation of methylene blue (the initial pH of MB solution was 6.3)

| | **Suspension pH** | **Primary particle size by DRX (nm)** | **Aggregate size by DLS (nm)** | **Accessible surface area for UV -calculated from aggregate size ($m^2.g^{-1}$)** |
|---|---|---|---|---|
| **$Ti(OH)_4$- 423 K** | 5.9 | 6 | 4500 | 0.35 |
| **$TiO_2$ - 573 K** | 5.7 | 12 | 400 | 3.85 |
| **$TiO_2$ - P25** | 5.7 | 25 | 350 | 4.40 |

*Photocatalytic activity evaluation*

Results of MB photocatalytic degradation tests are compared in figure 9a1. As expected, the amorphous powder #$Ti(OH)_4$ - 423 K clearly appears as the less efficient catalyst towards MB degradation.

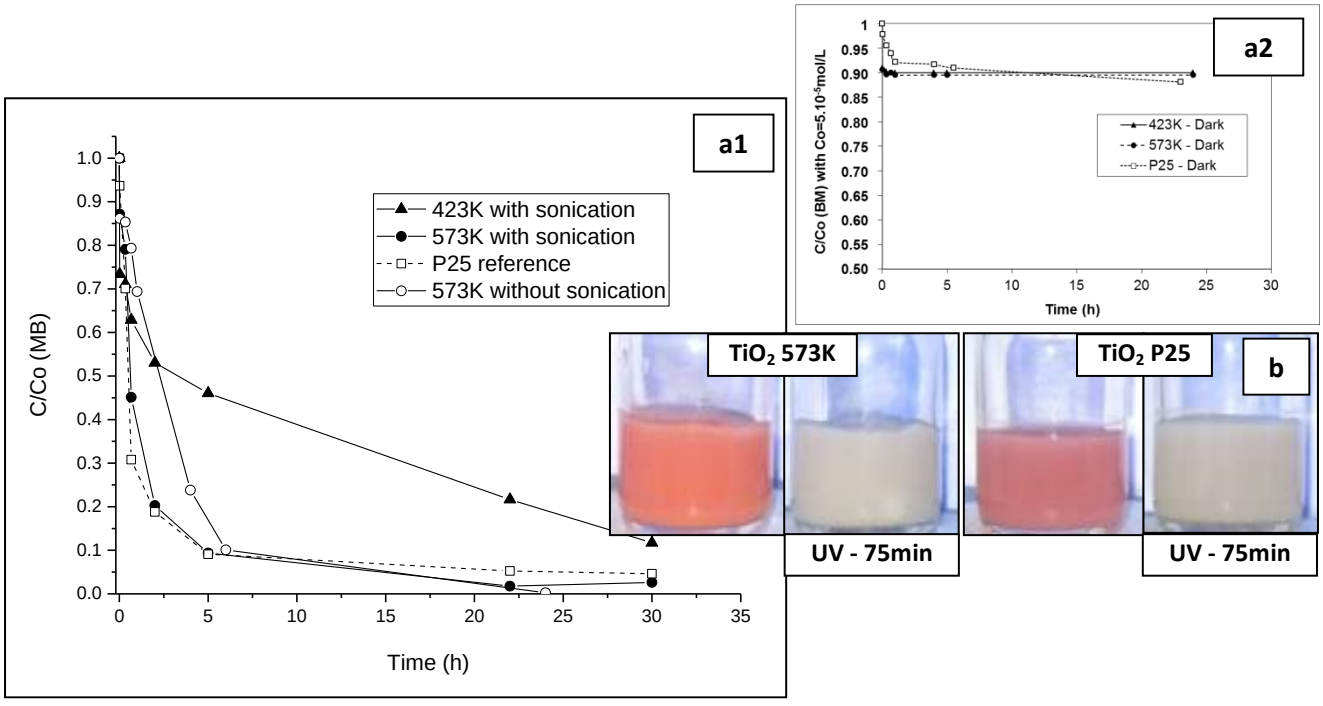


**Fig. 9** Photocatalytic performance of titania powders prepared at 423K and 573K in SC-$CO_2$, compared with commercial $TiO_2$ - P25, for the degradation of: a) methylene blue

solution ([MB] = 10 mg.$L^{-1}$ ; [$TiO_2$] = 0.2 g.$L^{-1}$) under UV (a1), or in dark conditions (a2), b) Congo red solution ([CR] = 15 mg.$L^{-1}$ ; [$TiO_2$] = 0.5 g.$L^{-1}$) in aqueous media under UV irradiation (Hg-UV lamp ; $\lambda$ = 365 nm).

The intrinsic sorption capacity of the nanostructured powders has been first evaluated without any UV lightning (dark conditions). If was found out that ~10 mol% of methylene blue was adsorbed on all the prepared $TiO_2$ powders after 24h treatment. Sorption kinetics were faster for the powders synthesized in SC-$CO_2$ in comparison with the P25 reference one, due to the high specific surface areas of the former.

Indeed, crystalline $TiO_2$ anatase is known to be the most efficient titania form in view of UV-light photocatalytic applications. Results obtained with the crystalline powder #$TiO_2$ – 573 K emphasize the role of powder/suspension conditioning on their photocatalytic efficiency. A suspension of #$TiO_2$ – 573 K powder merely dispersed in water by gentle stirring was less active than #$TiO_2$ - P25 suspension.

However, sonication-assisted dispersion (15 min in a lab-sonication bath) of #$TiO_2$ – 573 K powder was benefic to improve the photocatalytic perfomance and reach same efficiency and degradation kinetics as #$TiO_2$ - P25 suspension (figure 9a1). The powder surface accessible for UV irradiation is directly related to the size of primary particles, the size of aggregates and their dispersion degree. Hence, both the powder isoelectric point and the pH of the treated solution have a strong influence on the process efficiency, in addition to the structure, microstructure and design of the photocalyst.

Additional photocatalytic tests for the degradation of Congo Red dye (CR model molecule) proved the efficiency of #$TiO_2$ - 573 K (Figure 9b). A CR solution at 15 mg/L was completely cleaned in less than 75 min with 0.5 g.$L^{-1}$ #$TiO_2$ - 673 K, with degradation kinetics slightly better than those measured for #$TiO_2$ - P25.

## 4. Conclusion

A simple eco-friendly route for the preparation of titania nanopowders with well controlled and reproducible characteristics has been thoroughly described in this work. This green process, based on sol-gel processing of titanium isopropoxide ($Ti(O^iPr)_4$) and water as hydrolyzing agent in supercritical $CO_2$ (single supercritical phase), yields either submicronic titanium oxide ($TiO_2$ anatase) or titanium hydroxide spherical

particles, depending on the processing temperature. In fact, the low viscosity and high diffusivity of supercritical fluids counterbalance the low solvent power of supercritical $CO_2$ for polar compounds such as metal alkoxides. As a result, an inferred effect of the rapid diffusion and aggregation of nanoparticles in SC-$CO_2$ bears on the formation of spherical particles with a hierarchical microstructure. At low processing temperature (323 K), amorphous particles with sizes in the range 0.1 - 0.5 µm and high specific surface area (450 $m^2.g^{-1}$) were obtained. These particles transform to $TiO_2$ anatase by thermal treatment in air between 613 and 633 K. The rutile phase was formed between 1023 and 1123 K. Advantageously, it was possible to produce nanocrystalline spherical anatase particles directly in SC-$CO_2$, using a processing temperature ~ 523 K, i.e. lower than those typically required for the thermal crystallization of amorphous particles in air. The immediate benefits are a higher specific surface area of the powders and lower particle aggregation due to supercritical drying. It has demonstrated that the homogeneity of both particle sizes and microstructure has to be controlled by an appropriate choice of hydrodynamic parameters, namely reactant injection rate and stirring rate in the reactor. The as-prepared $TiO_2$ anatase powders synthesized in SC-$CO_2$ have a photocatalytic activity comparable to that of commercial P25 powder from Degussa. Moreover, the characteristics of these $TiO_2$ powders prepared under supercritical conditions are potentially attractive for a wide range of applications, e.g. catalyst support, chromatography static phase, pigment or ceramic membranes. Further investigations are currently in progress for studying their performance for the sorption of radionuclides or the photocatalytic degradation of biorefractory pollutants in liquid wastes.

**Acknowledgements**

The authors would like to thank Dr. Sébastien PAPET for his contribution to amorphous powder preparation and characterizations, M. Mickael GARCES and M. Damien AVRIL for their work on crystalline $TiO_2$ particles and Mlle Géraldine DIDERON for photo-catalytic tests.

The authors wish to confirm that there are no known conflicts of interest associated with this publication and there has been no significant financial support for this work that could have influenced its outcome.

**References**


1. Zhanga R., Elzatahryb A.A., Salem S. Al-Deyabb S.S, Zhao D., Mesoporous titania: from synthesis to application. Nano Today 7 (2012) 344-366.

2. Herrmann J.-M. Photocatalysis fundamentals revisited to avoid several misconceptions. Applied Catalysis B: Environmental 99 (2010) 461-468.

3. Fujishima A., Zhang X., Tryk D.A. $TiO_2$ photocatalysis and related surface phenomena. *Surface Science Reports* 63 (2008) 515-582.

4. Pelaez M., Nolanb N.T., Pillai S.C., Seeryc M. K., Falarasd P., Kontosd A.G., Dunlope P.S.M., Hamiltone J.W.J., Byrnee J.A., O'Sheaf K., Entezarig M.H., Dionysios D. Dionysioua D.D. A review on the visible light active titanium dioxide photocatalysts for environmental applications. Applied Catalysis B: Environmental 125 (2012) 331-349.

5. Bernardini C., Cappelletti G., Dozzi M., Selli E., Photocatalytic degradation of organic molecules in water: photoactivity and reaction paths in relation to $TiO_2$ particles features. J Photochem Photobiol A Chem 211:1 (2010) 85–92.

6. Lee K.-M., Hu C.-W., Chen H.-W., Ho K.-C., Incorporating carbon nanotube in a low-temperature fabrication process for dye-sensitized $TiO_2$ solar cells. Solar Energy Mater. Solar Cells, 92 (2008) 1628–1633.

7. Ding Z., Hu X., Lu G.Q., Yue P.-L., Greenfield P.F., Novel Silica Gel Supported $TiO_2$ Photocatalyst Synthesized by CVD Method. *Langmuir* 16 (2000) 6216-6222.

8. Lee B.I., Wang X., Bhave R., Hu M., Synthesis of brookite $TiO_2$ nanoparticles by ambient condition sol process. Materials Letters 60 (2006) 1179–1183.

9. Fang C.-S., Chen Y.-W., Preparation of titania particles by thermal hydrolysis of $TiCl_4$ in *n*-propanol solution. Materials Chemistry and Physics 78 (2003) 739–745.

10. Terada Y., Suzuki Y., Tohno S., Synthesis and characterization of $TiO_2$ powders by electrospray pyrolysis method. Materials Research Bulletin 47 (2012) 889–895.

11. Payakgul W., Mekasuwandumrong O., Pavarajarn V., Praserthdam P., Effects of reaction medium on the synthesis of $TiO_2$ nanocrystals by thermal decomposition of titanium (IV) n-butoxide. Ceramics International 31 (2005) 391–397.

12. Qourzal S., Assabbane A., Ait-Ichou Y., Synthesis of $TiO_2$ via hydrolysis of titanium tetraisopropoxide and its photocatalytic activity on a suspended mixture with activated carbon in the degradation of 2-naphthol. Journal of Photochemistry and Photobiology A: Chemistry 163 (2004) 317–321.

13. Beitollahi A., Daie A.H.H., Samie L, Akbarnejad M.M. Synthesis and characterization of mesoporous $TiO_2$ assembled as microspheres. Journal of Alloys and Compounds 490 (2010) 311–317.

14. Ding X.-Z., Liu X.-H., Synthesis and microstructure control of nanocrystalline titania powders via a sol-gel process. Materials Science and Engineering A224 (1997) 210-215.

15. Liu H., Yang W., Ma Y., Cao Y., Yao J., Zhang J., Tiandou HuT., Synthesis and characterization of titania prepared by using a photoassisted sol-gel method. Langmuir 19 (2003) 3001-3005.

16. Tanaka S., Daisuke Nogami D., Natsuki Tsuda N., Miyake Y., Synthesis of highly-monodisperse spherical titania particles with diameters in the submicron range. Journal of Colloid and Interface Science 334 (2009) 188–194.

17. Marugán J., Christensen P., Egerton T., Purnama H., Synthesis, characterization and activity of photocatalytic sol–gel $TiO_2$ powders. Applied Catalysis B: Environmental 89 (2009) 273-283.

18. Kaper H., Sallard S., Djerdj I., Antonietti M., Bernd M., Smarsly B.M., Toward a Low-Temperature Sol-Gel Synthesis of $TiO_2$ Using Mixtures of Surfactants and Ionic Liquids. Chem. Mater 22 (2010) 3502-3510.

19. Cheng Q.-Q., Cao Y., Yang L., Zhang P.-P., Wang K., Wang H.-J., Synthesis of titania microspheres with hierarchical structures and high photocatalytic activity by using nonanoic acid as the structure-directing agent. Materials Letters 65 (2011) 2833-2835.

20. Dittert B., Gavrilovi´c A., Schwarz S., Angerer P., Steiner H., Schöftner R., Phase content controlled $TiO_2$ nanoparticles using the MicroJetReactor technology. Journal of the European Ceramic Society 31 (2011) 2475–2480.

21. Farbod M., Khademalrasool M., Synthesis of $TiO_2$ nanoparticles by a combined sol–gel ball milling method and investigation of nanoparticle size effect on their photocatalytic activities. Powder Technology 214 (2011) 344-348.

22. Loryuenyong V., Angamnuaysiri K., Sukcharoenpong J., Suwannasri A., Sol–gel derived mesoporous titania nanoparticles: effects of calcination temperature and alcoholic solvent on the photocatalytic behavior. Ceramics International 38 (2012) 2233–2237.

23. Duvarci Ö. Ç., Çiftçioğlu M., Preparation and characterization of nanocrystalline titania powders by sonochemical synthesis. Powder Technology 228 (2012) 231–240.

24. Chhor K., Bocquet J.F., Pommier C., Syntheses of submicron $TiO_2$ powders in vapor, liquid and supercritical phases, a comparative study. Materials Chemistry and Physics 32 (1992) 249-254.

25. Gourinchas Courtecuisse V., Chhor K., Bocquet J.-F., Pommier C., Kinetics of the Titanium Isopropoxide Decomposition in Supercritical Isopropyl Alcohol. Ind. Eng. Chem. Res. 35 (1996) 2539-2545.

26. Zhang X., Heinonena S., Levänen E., Applications of supercritical carbon dioxide in materials processing and synthesis. RSC Adv. 4 (2014) 61137-61152.

27. Sanli D., Bozbag S.E., Erkey C., Synthesis of nanostructured materials using supercritical $CO_2$. Part I. Physical transformations Material Science, 47 (2012) 2995–3025.

28. Bozbag S.E., Sanli D., Erkey C., Synthesis of nanostructured materials using supercritical $CO_2$. Part II. Chemical transformations. J. Material Science, 47 (2012) 3469–3492.

29. Cansell F., Aymonier C., Design of functional nanostructured materials using supercritical fluids. J. Supercritical Fluids, 47 (2009) 508–516.

30. Sui R., Charpentier P., Synthesis of metal oxide nanostructures by direct sol–gel chemistry in supercritical Fluids. Chemical Review, 112 (2012) 3057–3082.

31. Tadros M.E., Adkins C.L.J., Russick E.M., Youngman M.P., Synthesis of titanium dioxide particles in supercritical $CO_2$. The Journal of Supercritical Fluids 9 (1996) 172-176.

32. Reverchon E., Caputo G., Correra S., Cesti P., Synthesis of titanium hydroxide nanoparticles in supercritical carbon dioxide on the pilot scale. J. of Supercritical Fluids 26 (2003) 253-261.

33. Stallings W.E., Lamb H.H., Synthesis of nanostructured titania powders via hydrolysis of titanium isopropoxide in supercritical carbon dioxide. Langmuir 19 (2003) 2989-2994.

34. Hong S.-S., Lee M.S., Lee G.-D., Lim K.T., Ha B.-J., Synthesis of titanium dioxides in water-in-carbon dioxide microemulsion and their photocatalytic activity. Materials Letters 57 (2003) 2975– 2979.

35. Alonso E., Montequi I., Lucas S., Cocero M.J., Synthesis of titanium oxide particles in supercritical $CO_2$: effect of operational variables in the characteristics of the final product. J. of Supercritical Fluids 39 (2007) 453-461.

36. Wakayama H., Fukushima Y., Supercritical $CO_2$ as a solvent for synthesis of nanoporous materials. Ind. Eng. Chem. Res. 39 (2000) 4641-4645.

37. Reverchon E., Adami R., Nanomaterials and supercritical fluids. J. of Supercritical Fluids 37 (2006) 1-22.

38. Zhou W., Li W., Wang J-Q., Qu Y., Yang Y., Xie Y., Zhang K., Wang L., Fu H., Zhao D., Ordered mesoporous black $TiO_2$ as highly efficient hydrogen evolution photocatalyst, J. Am. Chem. Soc. 26 (2014) 9280–9283.

39. Zhou W., Sun F, Pan K, Tian G, Jiang B., Ren Z, Tian C., Fu H., Well-ordered large-pore mesoporous anatase $TiO_2$ with remarkably high thermal stability and improved crystallinity: Preparation, characterization, and photocatalytic performance, Adv. Funct. Mater. 21 (2011) 1922.

40. Herrmann J.M., Heterogeneous photocatalysis: state of the art and present applications. Top Catal 34:1 (2005) 49-65.

41. Guillard C., Horikoshi S., Watanabe N., Hidaka H., Pichat P., Photocatalytic degradation mechanism for heterocyclic derivatives of triazolidine and triazole. Journal of Photochemistry and Photobiology A: Chemistry 149:1–3 (2002)155-168.

42. Carp O., Huisman C.L., Reller A., Photoinduced reactivity of titanium dioxide. Prog Solid State Chem 32:1–2 (2004) 33-177.

43. Bickley R.I., Gonzalez-Carreno T., Lees J.S., Palmisano L., Tilley R.J.D. A structural investigation of titanium dioxide photocatalysts. J Solid State Chem 92:1 (1991) 178-190.

44. Okamoto K-I., Yamamoto Y., Tanaka H., Tanaka M., Itaya A., Heterogeneous photocatalytic decomposition of phenol over $TiO_2$ powder. Bull Chem Soc Jpn 58:7 (1985) 2015-2022.

45. Munuera G., Rives-Arnau V., Saucedo A., Photo-adsorption and photo-desorption of oxygen on highly hydroxylated $TiO_2$ surfaces. Part 1.-Role of hydroxyl groups in photo-adsorption. Journal of the Chemical Society, Faraday Transactions 1: Physical Chemistry in Condensed Phases 75:0 (1979) 736-747.

46. Wiebe R., Gaddy V.L., Vapor phase composition of carbon dioxide-water mixtures at various temperatures and at pressures to 700 atmospheres. Journal of the American Chemical Society 63 (1941) 475-477.

47. Voorhees P.W., The theory of Ostwald ripening. Journal of Statistical Physics 38: 1/2 (1985) 231-252.

48. Edelson L.H., Glaeser A.M., Role of particle substructure in the sintering of monosized titania. Journal of the American Ceramic Society 71 (1988) 225-235.

49. Hertz A., Drobek M., Ruiz J.-C., Sarrade S., Guizard C., Julbe A., Robust synthesis of yttria stabilized tetragonal zirconia powders (3Y-TZP) using a semi-continuous process in supercritical $CO_2$. Chemical Engineering Journal 228 (2013) 622-630.

50. Klotz M., Marinha D., Guizard C., Julbe A., Addad A., Hertz A., Charton F., Sintering and conductivity of nano-sized yttria-doped $ZrO_2$ synthesized by a supercritical $CO_2$-assisted sol-gel process. Journal of Supercritical Fluids 115 (2016) 26-32.

51. Hertz A., Sarrade S., Guizard C., Julbe A., Synthesis and encapsulation of yttria stabilized zirconia particles in supercritical carbon dioxide. J. European Ceramic Society 26 (2006) 1195-1203.

52. Hertz A., Corre Y.-M., Sarrade S., Guizard C., Julbe A. Ruiz J.-C., Fournel B., Yttria Stabilized Zirconia Synthesis in Supercritical $CO_2$: Understanding of Particle Formation Mechanisms in $CO_2$ / Co-Solvent Systems. J. European Ceramic Society 30-7 (2010) 1691-1698.

53. Klotz M., Hernández W.Y., Guizard C., Viazzi C., Hertz A., Charton F., Tardivat C., Vernoux P., High specific surface area YSZ powders from a supercritical $CO_2$ process as catalytic supports for NOx storage-reduction reaction. Catalysis Science & Technology 5 (2015) 2125-2131.

54. J. Schneider J., M. Matsuoka M., M. Takeuchi M., J. Zhang J., Y. Horiuchi Y., M. Anpo M., D.W. Bahnemann D.W., Understanding $TiO_2$ Photocatalysis: Mechanisms and Materials. Chem. Rev. 114:19 (2014) 9919–998.

55. Lee S.-Y., Park S.-J., $TiO_2$ photocatalyst for water treatment applications. Journal of Industrial and Engineering Chemistry 19:6 (2013) 1761–1769.